

Article

On the Color and Genesis of Prase (Green Quartz) and Amethyst from the Island of Serifos, Cyclades, Greece

Stephan Klemme ^{1,*}, Jasper Berndt ¹, Constantinos Mavrogonatos ² , Stamatis Flemetakis ¹, Ioannis Baziotis ³, Panagiotis Voudouris ² and Stamatios Xydous ³

¹ Institut für Mineralogie, Westfälische Wilhelms Universität Münster, Corrensstrasse 24, 48149 Münster, Germany; jberndt@uni-muenster.de (J.B.); stam.flemetakis@uni-muenster.de (S.F.)

² Faculty of Geology and Geoenvironment, National and Kapodistrian University of Athens, 15784 Athens, Greece; kmavrogon@geol.uoa.gr (C.M.); voudouris@geol.uoa.gr (P.V.)

³ Laboratory of Mineralogy and Geology, Agricultural University of Athens, 11855 Athens, Greece; ibaziotis@aua.gr (I.B.); stxydous@aua.gr (S.X.)

* Correspondence: stephan.klemme@uni-muenster.de; Tel.: +49-(0)251-8333047

Received: 10 September 2018; Accepted: 24 October 2018; Published: 26 October 2018



Abstract: The color of quartz and other minerals can be either caused by defects in the crystal structure or by finely dispersed inclusions of other minerals within the crystals. In order to investigate the mineral chemistry and genesis of the famous prase (green quartz) and amethyst association from Serifos Island, Greece, we used electron microprobe analyses and oxygen isotope measurements of quartz. We show that the color of these green quartz crystals is caused by small and acicular amphibole inclusions. Our data also shows that there are two generations of amphibole inclusions within the green quartz crystals, which indicate that the fluid, from which both amphiboles and quartz have crystallized, must have had a change in its chemical composition during the crystallization process. The electron microprobe data also suggests that traces of iron may be responsible for the amethyst coloration. Both quartz varieties are characterized by isotopic compositions that suggest mixing of magmatic and meteoric/marine fluids. The contribution of meteoric fluid is more significant in the final stages and reflects amethyst precipitation under more oxidizing conditions.

Keywords: green quartz; prase; amethyst; color; amphibole; actinolite; skarn; Serifos; Greece

1. Introduction

Colored varieties of quartz (SiO₂) are ubiquitous in many igneous, metamorphic and sedimentary rocks [1–3]. They are well-loved collectors' items and comprise a number of semi-precious gems such as violet amethyst, yellow citrine, pinky rose quartz, and dark smoky quartz. Color in quartz is caused either by electronic defects of the crystal structure, transition metals or other elements incorporated in the crystal structure. Furthermore, color in quartz, and in other minerals, can also be caused by small, often nano-sized, well-dispersed mineral inclusions [3]. Blue quartz, pink rose quartz or jasper are known to be colored because of small inclusions of other minerals. Whilst it was thought for a long time that the color of rose quartz was caused by small rutile (TiO₂) inclusions, an electron microscopy study [4] showed that the rose quartz crystals from Montana, USA, contained small inclusions of dumortierite [(Al,Fe³⁺)₇(BO₃)(SiO₄)₃O₃]. Furthermore, there is evidence that other rose quartz types are colored by the incorporation of Mn, Ti or P in the quartz structure [3].

Compared to yellow, violet or pink quartz, green varieties of quartz are rare. There are some descriptions of natural green quartz which are commonly referred to as prasiolite [5,6]. However, most green prasiolite is prepared from natural amethyst by heating to 300–600 °C [7,8]. Some early studies found that

the color of green prasiolite quartz was caused by Fe^{2+} on an interstitial site in octahedral coordination within the quartz structure [2,9] but more recent studies using Mössbauer Spectroscopy questioned these results and concluded that the green color of prasiolite was caused by Fe^{3+} [6]. Detailed studies illustrate how color changes from amethyst to prasiolite during heating [3,7,8]. Rare natural examples of prasiolite have been reported from Reno, Nevada, USA [10] and Thunder Bay, Ontario, Canada [11,12].

Another green variety of quartz is commonly referred to as chrysoprase. The color of chrysoprase varies from olive-green to pale sea-green [3]. As far as we know, such chrysoprase has been described from Australian serpentinites [13] and jadeite-rich veins in lower Silesia [14]. Rossman concludes in his review [3] that the color of chrysoprase is caused by “fine-grained nickel compounds in the silicate matrix rather from substitutional Ni in the silica itself”. Possible Ni-minerals include bunsenite (NiO) or other complex hydrous Ni-silicates [3]. Recent studies of chrysoprase samples from Szklary (Poland) and Sarykul Boldy (Kazakhstan) showed that the “apple-green” color is caused by nano-scaled inclusions of Ni-kerolite and minor pimelite but they found no evidence for bunsenite inclusions [15]. Finally, Yang et al., [16] reported green quartzites (also known as “Guizhou Jade”) from the Quinglong antimony deposit, in the Guizhou province, China, and claimed that green coloration is due to the presence of Cr^{3+} - and V^{3+} -bearing dickite inclusions.

Amethyst, on the other hand, is a relatively common variety of quartz that forms in a wide variety of environments [17]. It is well known as a gemstone since antiquity, as it is mentioned by Theophrastus, the disciples of Aristotle (4th century B.C.). Amethyst comes in an attractive violet color with reddish or bluish tint, that was originally interpreted as a result of the presence of Fe^{3+} , which turns into Fe^{4+} after irradiation and substitutes for Si^{4+} in a deformed tetrahedral position [3]. However, recent studies, questioned this result and by using modern analytical techniques, like EPR, Mössbauer and synchrotron X-ray absorption spectroscopy attributed the coloration of amethyst in the presence of Fe^{3+} [6,18–20].

Amethyst is not very common in skarn deposits. When present, it is usually only of mineralogical interest, as it rarely comes in gem quality in this geological environment [21]. Amethyst has been described from the Fe-rich skarn deposits in Angara-Ilim in Russia [21,22]. Collector specimens of amethyst have been reported from the Dashkesan skarn deposit in Azerbaijan [21]. Sceptre-shaped amethyst crystals are also found in the skarns of Denny mountain, Washington, USA [21] and finally, amethyst crystals have also been found in Hässellkulla, Sweden, in the Örebro Fe-rich skarn deposit [21,23,24].

Here we will present some results of an electron microprobe and oxygen isotope study on green quartz crystals and associated amethyst from the skarn of Serifos Island in Greece, which comprises, to our knowledge, the only locality that produces specimens with both quartz varieties. These green quartz and amethyst crystals are well known to collectors and fetch rather high prices during auctions [25,26]. However, not much is known about the origin of these quartz crystals or the origin of the green color in Serifos quartz. Similar-looking green quartz crystals are available for sale from internet mineral dealers and are sourced from Dalnegorsk, Russia [27]. As to the color, there are, to our knowledge, no peer-reviewed articles that investigated the nature of the green Serifos or similar green quartz crystals in any detail. Hyrsl and Niedermayr [28] reported actinolite from XRD analyses of prase from Serifos, but presented no further analytical data. Similarly, Maneta and Voudouris [29] reported actinolite inclusions to be responsible for the green color of quartz from Serifos, and Voudouris and Katerinopoulos [30] described similar green quartz crystals from the skarn occurrences at the Xanthi and Kresti/Drama areas in northern Greece, but without any detailed analytical data. Some recent published studies suggested inclusions of hedenbergite as potential candidates that may be responsible for the color of green quartz crystals in Serifos quartz [27,31].

2. Materials and Methods

We analyzed representative cm-sized prismatic crystals of prase (green quartz), and amethyst. To characterize both the quartz varieties and to search for possible mineral inclusions, we used optical microscopy and electron microprobe analyses (EMPA). Electron microprobe analyses on prase and its

inclusions were performed with a JEOL 8530F field emission microprobe at the University of Münster (Germany). This microprobe enables us to take high-resolution back-scattered electron images and also to analyze small crystals with high accuracy. Analytical conditions for amphiboles were 15 kV accelerating voltage, 15 nA beam current, 5 μm spot size, and counting times of 10 s for peak and 5 s for the background signal except for Na and K (5 s for peak and 2 s for background). Prior to quantitative analyses all elements were standardized on matrix matched natural (Na, Mg, K, Si, Al, Ca, Fe, Mn) and synthetic (Ti, Cr) reference materials. Although quartz is known to be a robust mineral in regards to structure, hardness and weathering, it is nevertheless very sensitive to electron irradiation. Thus, special care must be taken analyzing quartz and its trace elements like Al, Fe, Ti, and K. We followed a recently published analytical protocol [32] using a beam current of 80 nA at 15 kV, 60 s peak and 30 s background counting time with a probe diameter of 15 μm . A blank quartz sample was measured along with the unknowns in order to check for “true-zero” concentrations. The average detection limits (3σ) for Al, K, Ti, and Fe is in the range of 0.011 wt % oxides. The phi-rho-z correction was applied to all data. To monitor accuracy and precision over the course of this study micro-analytical reference materials were analyzed and obtained results match published values within error.

Amethyst in polished sections embedded in resin, was analyzed using a JEOL JXA 8900 Superprobe equipped with four wavelength-dispersive spectrometers (WDS) and one energy-dispersive spectrometer (EDS) at the Agricultural University of Athens (Greece). All analyses were performed with an accelerating voltage of 15 kV, 15 nA beam current, slightly defocused beam (2 μm), 20 s counting time on peak position and 10 s for each background. Natural mineral standards used were jadeite (Na), quartz (Si), corundum (Al), diopside (Ca), olivine (Mg), fayalite (Fe), spessartine (Mn), microcline (K), ilmenite (Ti), chromite (Cr), apatite (P) and Ni-oxide (Ni).

Stable isotope analyses were performed at the Stable Isotope and Atmospheric Laboratories, Department of Geology, Royal Holloway, University of London (UK). The oxygen isotope composition of quartz was obtained using a CO₂ laser fluorination system similar to that described by Matthey [33]. Each mineral separate is weighed at 1.7 mg \pm 10%. These were loaded into the 16-holes of a nickel sample tray, which was inserted into the reaction chamber and then evacuated. The oxygen was released by a 30 W Synrad CO₂ laser in the presence of BrF₅ reagent. The yield of oxygen was measured as a calibrated pressure based on the estimated or known oxygen content of the mineral being analyzed. Low yields result in low $\delta^{18}\text{O}$ values for all mineral phases, so accurate yield calculations are essential. Yields of >90% are required for most minerals to give satisfactory $\delta^{18}\text{O}$ values. The oxygen gas was measured using a VG Isotech (now GV Instruments, Wythenshawe, UK) Optima dual inlet isotope ratio mass spectrometer (IRMS). All values are reported relative to the Vienna Standard Mean Ocean Water (V-SMOW). The data are calibrated to a quartz standard (Q BLC) with a known $\delta^{18}\text{O}$ value of +8.8‰ V-SMOW from previous measurements at the University of Paris-6 (France). This has been further calibrated for the RHUL laser line by comparison with NBS-28 quartz. Each 16-hole tray contained up to 12 sample unknowns and 4 of the Q BLC standard. For each quartz sample a small constant daily correction, normally less than 0.3‰, was applied to the data based on the average value for the standard. Overall, the precision of the RHUL system based on standard and sample replicates is better than $\pm 0.1\%$.

3. Geological Setting

Serifos Island is located in the NW edge of the Cyclades Island complex. In the Cyclades area, three major tectono-metamorphic units have been distinguished, namely the Cycladic Continental Basement Unit (CCBU), the Cycladic Blueschists Unit (CBU) and the Upper Cycladic Unit (UCU) [34–37].

Serifos is occupied by a metamorphic sequence which comprises [38–40]: (a) a basal gneiss, mylonitic schists and marbles unit, with a maximum thickness of about 200m, that has been interpreted as member of the CCBU; (b) an intermediate rock unit made of amphibolites and overlying greenschists with rare marble intercalations, occupying the northern part of the Island and containing relics of glaucophane, that are typical of the CBU [41]; (c) and finally, an uppermost unit with marbles,

ankeritised protocataclastic shales and minor serpentinite [31]. Contacts between the rock units are marked by tectonic structures (Figure 1), namely the Megalo Livadi and Kavos Kyklopas detachment faults, which belong to the West Cycladic Detachment System, (WCDS [42]) and are characterized by top-to-the SSW kinematics on the footwalls.

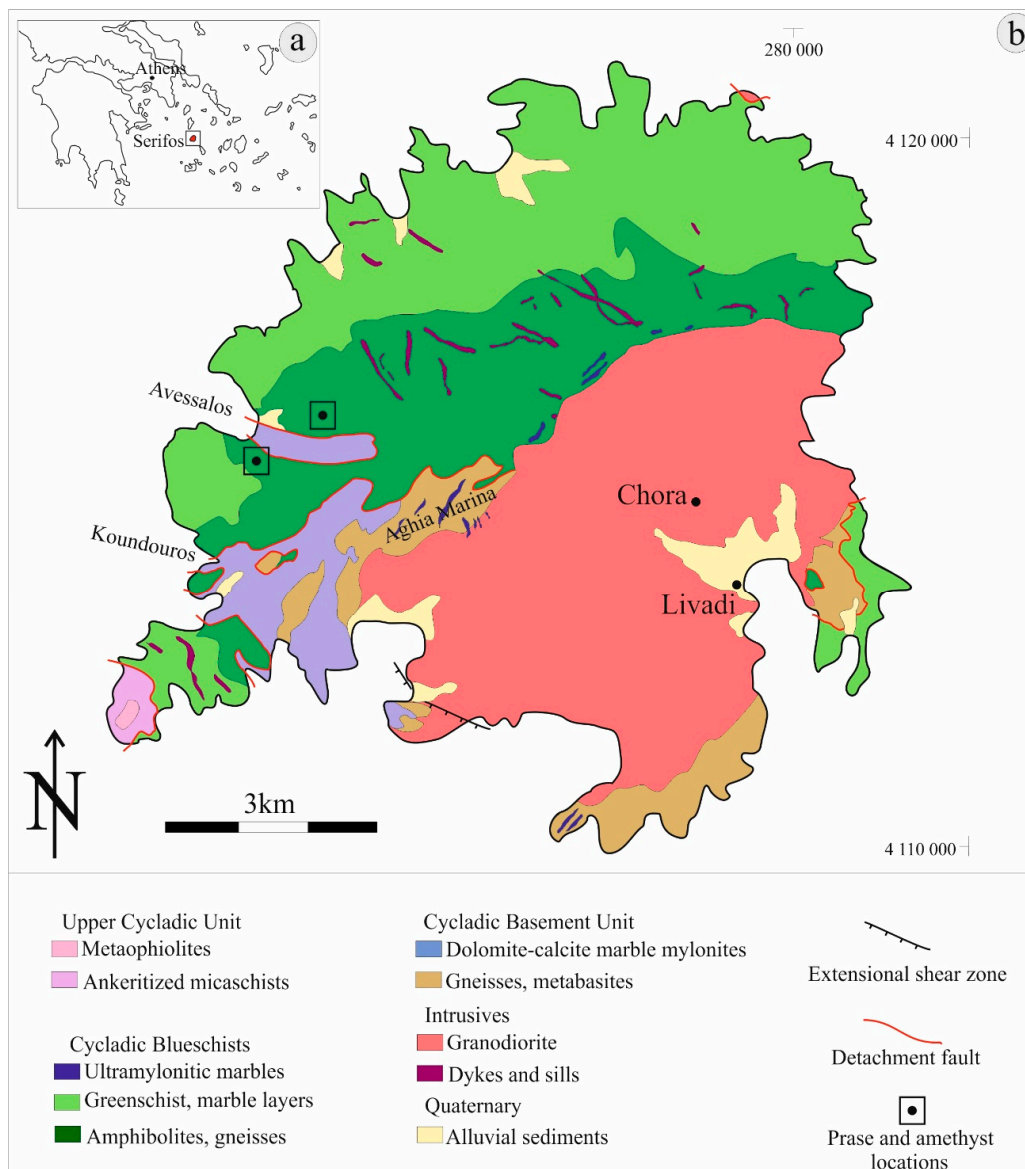


Figure 1. (a) Serifos Island is located in the NW edge of the Cyclades Island complex in the Aegean Sea, Greece. (b) Simplified geological map of Serifos Island (modified after Ducoux et al. [31]). Black squares indicate the study areas of Avessalos (South) and Neroutsika (North).

The above-mentioned rock units are intruded by an I-type, hornblende-biotite granodiorite which displays two variants [43]: the inner part of the intrusion comprises a fine-grained equigranular, unfoliated rock, while the outer part is composed of a coarse-grained equivalent, characterized by large biotite flakes and mafic enclaves. Many dykes and sills of granodiorite, microgranite and rhyodacite/dacite are scattered around the intrusion [44].

A number of skarns have formed close to the granodiorite intrusion [39–41,43] and have been long known for their Fe-rich mineralisation, that was exploited until the 1960's. Mines are widespread over the Island and were targeted at magnetite-rich skarn zones or in hematite/limonite±barite orebodies in marbles [31]. These skarns are also the general area where the unique Serifos green quartz,

mostly known as prase (or prasem), is found (Figure 2). Except for the well-known green quartz, a great variety of other aesthetic minerals can also be found in the skarn zones of Serifos [25].



Figure 2. Field and prase/amethyst specimen photographs: (a); The Avessalos location (view towards SW), famous for its prase; (b) The Neroutsika location (view towards NE) from where unique combinations of prase with amethyst were recovered (Figure 2g); (c) Geode within hedenbergitic skarn, filled with euhedral prase crystals, Avessalos locality; (d,e) aesthetic prase crystals combinations from Avessalos locality; (f) negative scepter, formed by an upper part of amethystine quartz that grows atop a basal part of prase, Avessalos locality; (g) bi-colored crystal consisting of a basal prase part and an upper amethyst part of gem quality, Neroutsika locality. Figures and specimen 3d and 3e–f are courtesy of C. Mavrogonatos and P. Voudouris respectively.

Among them, ilvaite, a rare sorosilicate mineral is mainly found in Koundouros area, which is located a few kilometers north from Avessalos. Samples from this locality, are considered to be among the best of its kind.

Andraditic garnets, often zoned are found in euhedral translucent crystals on top of hedenbergite in geodes with varying dimensions in the areas of Avessalos and Agia Marina. Finally, tabular translucent

barite and rhombohedral calcite have been found in exceptional crystals in places close to the Fe-rich mineralization [25,30].

The green quartz from Serifos is usually translucent, with a characteristic green color in different intensities. Typical are cigar-shaped crystals which extend from a fine-grained matrix consisting of hedenbergite. Often smaller crystals sprout from the prism of larger crystals, resulting in very aesthetic aggregates. Green quartz is extracted from a few localities in the SW part of Serifos Island. The most important of these are the localities of Avessalos (Figures 1 and 2 and Neroutsika (Figures 1 and 2b). Our samples are from the western part of Serifos (Figure 1), within amphibolite facies rocks and the skarn mineralization [25,26,29,30].

Minor green quartz occurrences can also be found in Agia Marina and Koundouros. The studied samples come from the well-known locality of Avessalos (Figure 2a,c–f), from where the best green quartz samples have been found. Crystals from this site are usually lustrous with vivid green color, in contrast to other sites, from where green quartz is usually not translucent, but with varying intensity of its green color. Green quartz is often found in geodes between brecciated, up to tens of meters-sized blocks of skarnified amphibolites [25,26,29,30]. Brecciation of the amphibolites has been caused by the activation of the WCDS and created pathways through which hydrothermal fluids arising from the granodiorite created the widespread skarns on the Island [31].

Empty spaces between the more-or-less skarnified amphibolite blocks, commonly occur in triangular shapes that may vary significantly in size (Figure 2c), sometimes reaching a width of a few meters across. These spaces are filled by hedenbergite, followed by ilvaite, prase ± amethyst, hematite and carbonate (calcite) deposition towards the centre of the open spaces. Inside these geodes, the prase (green quartz) crystals develop in a variety of crystals shapes. Figure 2d–g displays some aesthetic aggregates with sharply terminated crystals, sceptres and reverse sceptres of prase combined with amethyst from both Avessalos and Neroutsika areas. In many cases, prase is accompanied by calcite and iron-roses composed of hematite [25,26]. Its crystal shape is usually spindle-like in the basal part and evolves into hexagonal on the top of the crystal. Prismatic green quartz crystals are also found, as well as bi-colored, rocket-like shapes, with amethyst in the base and green quartz on top. The sceptres found in the area are normal or inverse with green quartz in the base and an often trigonal amethystine termination (Figure 2f–g). An unusual type of crystals encountered in the area is the “interrupted” prase or amethyst crystals which form when platy calcite crystals are deposited together with quartz in successive layers [21,26].

4. Results

4.1. Mineral Chemistry

Detailed microscopy and back-scattered electron (BSE) images reveal that the Serifos green quartz contains numerous small inclusions. We find two general types of mineral inclusions. The first type comprises myriads of acicular amphibole crystals which are often 10–100 µm long, but their thickness is limited to below a few µm. These thin actinolite needles are practically found everywhere and seem to be randomly oriented. We did not observe any obvious relationship between amphibole orientation and the crystallographic orientation of the quartz crystals. Some of the needles (Figure 3a,b) are clearly curved, a fact that supports random orientation of the amphibole needles in relation to the host quartz crystals. With our electron microprobe we could only identify the needles as actinolitic amphibole but accurate analysis was not possible, due to the small size of the inclusions. We, therefore, assume that the chemical compositions of these thin amphibole needles are identical to the rims of the larger amphibole inclusions, a fact that also seems to be supported by electron microprobe maps (Figure 3e–f).

The second type consists of larger inclusions (Figure 3a–c) with sizes that reach a few tens of µm in length (commonly between 10 and 60 µm), and that always display zonation. EPMA analyses revealed that these inclusions are Ca-Fe-rich actinolitic amphiboles with compositions very close to the end-member

ferro-actinolite. These minerals contain about 5 wt % MgO, almost no Na or K, and about 2 wt % Al₂O₃. All the studied larger actinolite inclusions contain a core, which is significantly lighter in BSE images. Microprobe analyses (Table 1) reveal that these cores are also actinolite, with some differences compared to the rims. MnO content is almost doubled compared to the rim (0.56 and 0.25 wt % respectively) and FeO is slightly higher. Subsequently, the cores contain lower MgO and (3.8 wt %) and much less Al₂O₃ (0.3 wt %).

Table 1. Electron microprobe measurements of amphibole inclusions, prase and amethyst from Serifos Island.

n.o.a.	Amphibole					Prase		Amethyst	
	3 (core)		6 (rim)			11		14	
	wt %	2σ	wt %	2σ		wt %	2σ	wt %	2σ
SiO ₂	51.1	0.04	50.6	0.57		99.3	0.56	99.9	0.44
TiO ₂	0.05	0.00	0.01	0.02		-	-	0.005	0.01
Al ₂ O ₃	0.38	0.01	1.54	0.57		0.26	0.12	0.123	0.11
Cr ₂ O ₃	n.a.	-	n.a.	-		n.a.	-	0.006	0.01
FeO	29.4	0.40	28.3	1.15	Fe ₂ O ₃	0.027	0.019	0.021	0.03
MnO	0.56	0.02	0.25	0.12		n.a.	-	0.006	0.01
MgO	3.81	0.07	4.98	0.72		n.a.	-	0.01	0.01
CaO	11.6	0.04	11.3	0.09		n.a.	-	0.008	0.01
Na ₂ O	0.03	0.02	0.26	0.11		n.a.	-	0.01	0.01
K ₂ O	0.09	0.02	0.19	0.05		0.008	0.007	0.006	0.01
P ₂ O ₅	n.a.	-	n.a.	-		n.a.	-	0.012	0.02
Total	96.9		97.5			99.6		100.2	
Structural formulae									
Si	8.08		7.85		Si	0.998		0.998	
AlVI	0.00		0.15		Ti	0.000		0.000	
M1-3 site					Al	0.003		0.000	
AlVI	0.07		0.13		Fe ³⁺	0.000		0.0002	
Ti	0.01		0.00		Mn	-		-	
Fe ³⁺	0.00		0.13		Mg	-		0.000	
Mg	0.89		1.15		Ca	-		-	
Fe ²⁺	3.87		3.55		Na	-		-	
Mn	0.08		0.03		K	0.000		-	
Σ					P	-		0.000	
M1-3 site	4.92		5.00		Σ All	1.001		1.009	
M4 site									
Mg	0.00		0.00						
Fe ²⁺	0.00		0.00						
Mn	0.00		0.00						
Ca	1.95		1.88						
Na	0.01		0.08						
Σ M4 site	1.96		1.96						
A site									
Na	0.00		0.00						
K	0.02		0.04						
Σ A site	0.02		0.04						
Σ All	15.0		15.0						

n.a. = not analysed; (-) = below detection, n.o.a. = number of analyses.

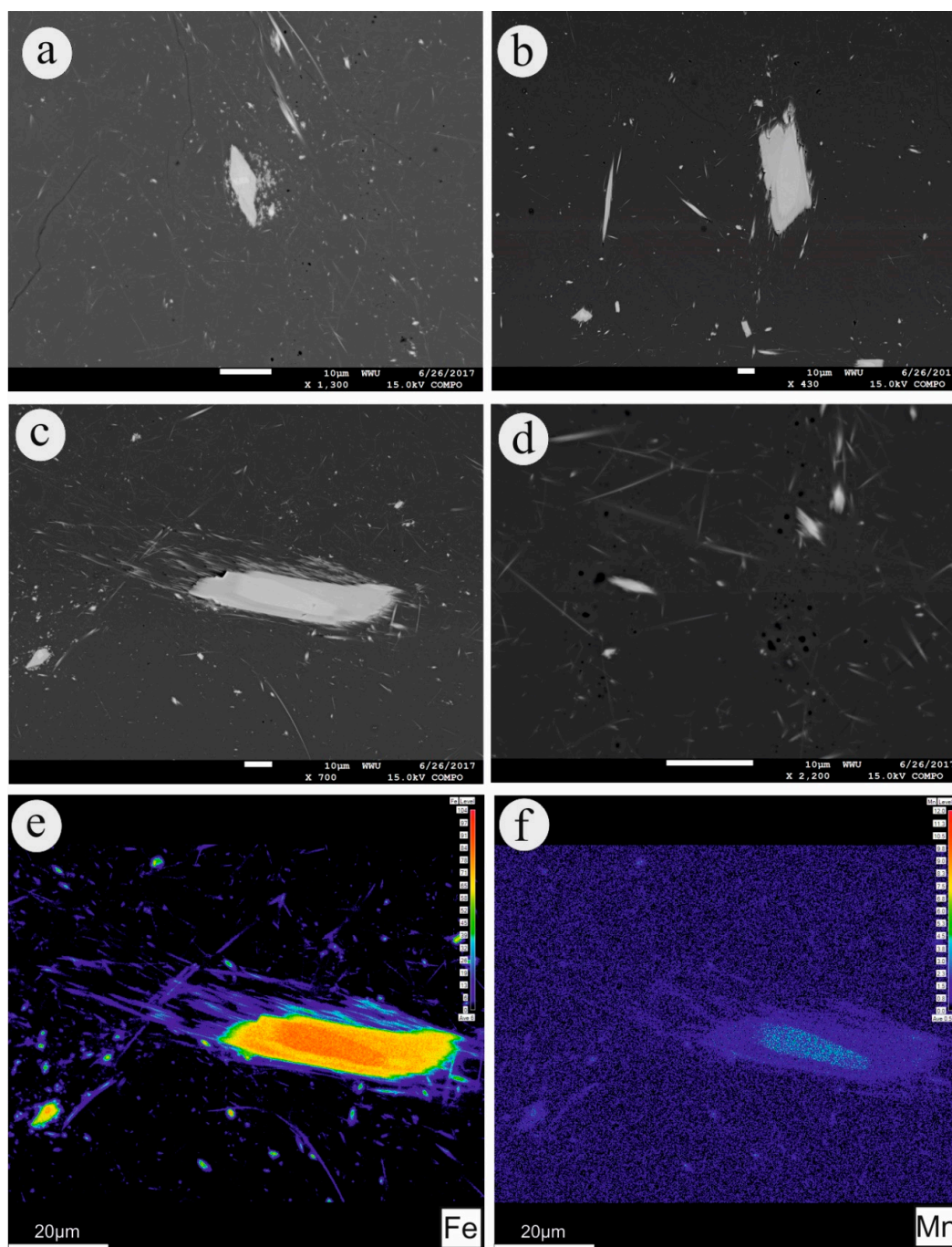


Figure 3. Back-scattered electron (BSE) images and quantitative electron microprobe element maps. (a): thin, nm-sized needles of amphibole together with a larger amphibole. The latter larger actinolite contains a core of more calcic actinolite; (b) Large amphibole with no clearly defined edges, as the rapid growth of the crystal has stopped. Furthermore, it seems that this amphibole has already determined the outer edge of the crystal which it would have grown into if growth had not been interrupted. The origin of the observed textures is unknown; (c) Similar larger amphibole with a fringed edge also indicating rapid growth; (d) high-resolution image of the fine-grained matrix. The dark blebs are empty and are interpreted as fluid inclusions that were opened during sample preparation; (e) Quantitative electron microprobe map of Fe. The cores of the larger amphiboles contain significantly more FeO (Table 1) than the rims. The color bar on the right-hand side indicates chemical composition (wt % FeO). Note that the very thin needle-shaped (blueish in this Figure) actinolite crystals are too small to be analyzed so that the FeO-content is underestimated; (f) Quantitative electron microprobe map of Mn. The cores contain significantly more Mn than the rim actinolite, indicating two different generations of amphibole.

The CaO content is quite similar in both rim and core with values around 11.5 wt %. Finally, traces of Na₂O and K₂O were detected in both rim and core actinolites. Values for both elements increase towards the rims of the crystals, reaching values of up to 0.26 and 0.19 wt % respectively. Average chemical formulae for the compositions from the cores and the rims of the crystals correspond to [Ca_{1.95}Na_{0.01}K_{0.02}]_{1.98} [Mg_{0.89}Fe²⁺_{3.87}Mn_{0.08}Al_{0.07}Ti_{0.01}]_{4.92} [Si]_{8.08} O₂₂(OH)₂ and [Ca_{1.88}Na_{0.08}K_{0.04}]₂ [Mg_{1.15}Fe²⁺_{3.55}Fe³⁺_{0.13}Mn_{0.03}Al_{0.13}]_{4.99} [Si_{7.85}Al_{0.15}]₈ O₂₂(OH)₂, respectively. Analytical data from prase and amethyst yielded traces of Al₂O₃, FeO, MgO, MnO, CaO, Na₂O, K₂O and P₂O₅. The highest FeO and Al₂O₃ contents were found in prase (up to 0.26 and 0.024 wt % respectively). Amethyst Fe₂O₃ content reaches up to 0.020 wt % (calculated from the total FeO of the analyses).

4.2. Quartz Oxygen Isotopes

The quartz oxygen isotopic compositions were analyzed in hand-picked prase and amethyst crystals. The compositions of the fluid in equilibrium with the prase and amethyst crystals were calculated following Sharp et al. [45], using temperatures of 350 °C for prase and 250 °C for amethyst, based on the respective mineral assemblages of Salemink [43].

The studied prase samples yielded isotopic $\delta^{18}\text{O}_{\text{Qz}}$ values of 12.72 and 12.74‰, which correspond to calculated $\delta^{18}\text{O}_{\text{Fl}}$ values of 7.32 and 7.14‰ (Table 2). Amethyst samples yielded $\delta^{18}\text{O}_{\text{Qz}}$ values of 9.94 and 9.85‰, which correspond to calculated $\delta^{18}\text{O}_{\text{Fl}}$ values of 1.04 and 0.95‰ respectively. The isotopic signature of prase is comparable to those of quartz samples from different assemblages of the skarn zone, but amethyst displays significantly lighter isotopic signature (Figure 4).

Table 2. Oxygen isotope compositions of quartz from the skarn of Serifos Island [δ values in‰ relative to Standard Mean Ocean Water (SMOW)]. The oxygen isotope values in the fluid ($\delta^{18}\text{O}_{\text{Fl}}$) in equilibrium with quartz have been calculated according to Sharp et al., [45].

Sample	Variety	Associated Minerals	$\delta^{18}\text{O}_{\text{Qz}}$	T (°C)	$\delta^{18}\text{O}_{\text{Fl}}$
SR2a	prase	ac	12.72	350	7.32
SR2b	prase	ac	12.54	350	7.14
SR1a	amethyst	hem	9.94	250	1.04
SR1b	amethyst	hem	9.85	250	0.95
20–11 *	quartz	ep	11.4	400	6.8
27–30 *	quartz	ep	12.6	400	8.0
26–49 *	quartz	Mt + hem	11.6	410	7.2
26–48 *	quartz	Mt + hem	12.3	400	7.7
26–87 *	quartz	Ep + ac	13.3	405	13.3
137 *	quartz	Ac + cc	14.7	390	14.7
55 *	quartz	iv	12.6	350	6.8
55-(1) *	quartz	iv	12.5	325	6.0
56 *	quartz	iv	13.2	325	6.7
26–35 *	quartz	mt	14.4	325	7.8
ML-2.2 *	quartz	Ac + mt	16.6	265	7.8
ML-1 *	quartz	Ac + mt	16.5	260	7.5
27-7B *	quartz	Py + hem + cc	14.8	250	5.2

Samples marked with (*) are from Salemink [43]. Abbreviations: ac = actinolite; hem = hematite; ep = epidote; mt = magnetite; iv = ilvaite; cc = calcite; py = pyrite.

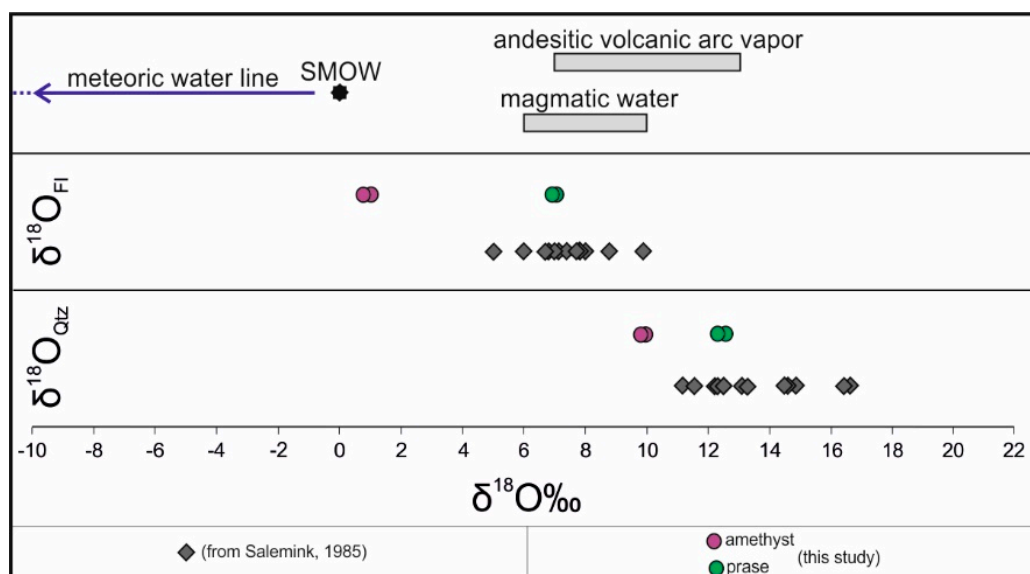


Figure 4. $\delta^{18}\text{O}$ values of quartz from the skarn of Serifos Island, Greece. Values for magmatic water and andesitic volcanic arc vapor are from Taylor [46] and Giggenbach [47] respectively.

5. Discussion

Prase or prasem, a green-colored variety of quartz has been long known to collectors because of its rarity, compared to other colorful varieties. Worldwide, the occurrences of natural green quartz are only a few [6].

Among them, prase crystals from the Island of Serifos are believed to be the best of its kind. In rare cases, amethyst, that grows on top of a basal part of prase, creates a unique combination of these two quartz varieties that has not been described elsewhere than Serifos. Despite its high collective and commercial value, little research has been carried about what causes the green color and how this rare variety of quartz is formed together with amethyst in the skarn zones of Serifos. In addition, there is some information in the older literature on color caused by defects in quartz, summarized in an excellent review paper by Rossman [3], but there is very little modern data on the chemical and mineralogical composition of inclusions in quartz in general, and not only in the case of green quartz from Serifos Island.

The majority of previous studies suggested that the color of the Serifos green quartz was caused by hedenbergite-rich pyroxene inclusions (e.g., [27,31]), and only Hyrsl and Niedermayr [28] reported actinolite, based on XRD analyses, but did not present any analytical data. Our new data suggests that it is indeed amphiboles which are responsible for the typical green color. To our knowledge, these are the first quantitative measurements of amphibole inclusions in green quartz and first quantitative data to explain the cause of the color of green quartz from Serifos Island.

Acicular and needle-shaped actinolite inclusions are scattered throughout the quartz crystals. Two types of inclusions were found: a plethora of very small (nanometer-sized) actinolites and a smaller number of larger, chemically zoned actinolite crystals, both without any obvious orientation in relation to the crystallographic orientation of the host quartz crystals.

Chemical analyses suggest that the cores of the larger actinolites is chemically different from the rims, the latter of which are of a similar chemical compositions compared to the very small acicular inclusions. All the larger actinolite inclusions exhibit typical amphibole crystal shapes, but often crystal faces are not well developed. In some cases, amphibole crystals are characterized by fuzzy crystal faces or fringed edges, likely indicating very rapid growth, which has been interrupted probably during rapid depressurization of the fluid-filled vein. This is a process which is typical for pegmatitic veins in which pressure drops rapidly during crack formation and, as a consequence, precipitation of the solutes. In the case of the Serifos green quartz, we surmise that the precipitation of the core

actinolites must have happened before the main event, in which the rim actinolite and the quartz itself crystallized. Whilst the core amphibole could have grown relatively slowly from the fluid, the crystallization of the actinolite needles and the overgrowth rim amphibole must have happened very fast indeed. Rapid depressurization and non-equilibrium conditions are in accordance with boiling conditions in the geodes, as suggested by the presence of platy calcite, which is intergrown with prase and amethyst [30,48].

In addition, we identified traces of iron using electron microprobe measurements of the Serifos green quartz which could also contribute to the green color, as suggested by Lehmann and Bambauer [2], Henn, Schultz-Guttler [9] and Czasa et al., [6]. On the other hand, traces of iron, found in amethyst from the same localities are the only impurity that could justify the light violet color of Serifos' amethysts. Our EPMA data revealed a mean content of 0.02 wt % Fe₂O₃, a quantity that is thought to be sufficient to justify the pale violet color of the studied crystals [49].

Previous stable isotope studies revealed a significant contribution of magmatic water for most of the samples of quartz that were studied by Salemink [43]. Oxygen isotopic values in prase are comparable to those of (colorless and milky) quartz, but display a trend towards lighter isotopic signature, which probably corresponds to the evolution of the skarn in its final stages. We find evidence for a major contribution of meteoric (and/or marine) water in case of the amethysts, thus recording a transition to more oxidizing conditions, as the formation of amethyst goes together with incorporation of Fe³⁺ [3] into its structure. The required oxidizing conditions were probably a result of mixing oxidized meteoric or marine water with upwelling hydrothermal fluids [50,51]. Amethyst was deposited in the final stages of the skarn, at temperatures around 250 °C. This is in good agreement with Kievlenko [21], who stated that amethyst in garnet-pyroxene-magnetite skarn deposits crystallizes in late or re-opened fractures and cavities.

Formation of prase and especially amethyst, is therefore, likely to be temporally related to the final stages of the Serifos' skarn, which according to Ducoux et al. [31], is contemporaneous with the intrusion of the granodiorite and the extensional deformation along the West Cycladic detachment system.

6. Conclusions

We conclude that the green color of the Serifos green quartz is caused by nano- to micrometer-sized actinolite inclusions. We find two generations of actinolite crystals, with the earlier and larger actinolite inclusions containing less MgO (and consequently more FeO) and Al₂O₃, but more MnO compared to the later acicular actinolite, which is rimming the earlier larger crystals. Average chemical formulae correspond to [Ca_{1.95}Na_{0.01}K_{0.02}]_{1.98} [Mg_{0.89}Fe²⁺_{3.87}Mn_{0.08}Al_{0.07}Ti_{0.01}]_{4.92} [Si]_{8.08} O₂₂ (OH)₂ for the early cores and [Ca_{1.88}Na_{0.08}K_{0.04}]₂ [Mg_{1.15}Fe²⁺_{3.55}Fe³⁺_{0.13}Mn_{0.03}Al_{0.13}]_{4.99} [Si_{7.85}Al_{0.15}]₈ O₂₂ (OH)₂ for the rims, respectively. The color of Serifos' amethysts is caused of the presence of trace Fe³⁺. Our conclusions highlight the need for further microanalytical data of quartz crystals, regardless of the color, in order to better understand the procedures under which this unique mineralogical assemblage of Serifos Island was generated. The existence two different generations of actinolite could be used to monitor the chemical composition of the fluids from which the amphibolites and the quartz crystals in the geodes were formed. Future work should include other analytical techniques (e.g., Mössbauer spectroscopy, LA-ICP-MS, EPR etc.) that could also help to define the cause of the green color in prase and amethyst. Moreover, fluid inclusions studies in all quartz varieties from the Serifos Island skarn deposits, should be conducted, as to monitor temperature and salinity of the skarn-forming fluids.

Author Contributions: C.M. collected the samples. J.B. assisted by S.F., I.B. and S.X., evaluated the mineralogical data. P.V. and C.M. evaluated the isotopic analyses. S.K., C.M. and P.V. wrote the manuscript.

Funding: This project was partially funded by a DAAD/IKY Program between University of Münster and the Agricultural University of Athens.

Acknowledgments: The authors wish to thank M. Trogisch at Münster University for preparation of the thin sections and B. Schmitte for her help with the EMPA measurements Two anonymous reviewers are thanked for their constructive comments on the manuscript.

Conflicts of Interest: The authors declare no conflict of interest.

References

- Hutton, D. Defects in the coloured varieties of quartz. *J. Gemmol.* **1974**, *14*, 156–166. [[CrossRef](#)]
- Lehmann, G.; Bambauer, H.U. Quarzkristalle und ihre Farben. *Angew. Chem.* **1973**, *85*, 281–289. [[CrossRef](#)]
- Rossmann, G.R. Coloured Varieties of the Silica Minerals. *Rev. Mineral.* **1994**, *29*, 433–467.
- Applin, K.R.; Hicks, B.D. Fibers of Dumortierite in quartz. *Am. Mineral.* **1987**, *72*, 170–172.
- Chauhan, M. Prasiolite with inclusion influenced by Brazil-law twinning. *Gems Gemol.* **2014**, *50*, 159–160.
- Czaja, M.; Kaździołka-Gawęł, M.; Konefał, A.; Sitko, R.; Teper, E.; Mazurak, Z.; Sachanbiński, M. The Mossbauer spectra of prasiolite and amethyst crystals from Poland. *Phys. Chem. Miner.* **2017**, *44*, 365–375. [[CrossRef](#)]
- Neumann, E.; Schmetzer, K. Farbe, Farbursache und Mechanismen der Farbumwandlung von Amethyst. *Zeitschrift der Deutschen Gemmologischen Gesellschaft* **1984**, *33*, 35–42.
- Neumann, E.; Schmetzer, K. Mechanism of thermal-conversion of colour and colour-centers by heat treatment of amethyst. *N. Jahrb. Miner. Monatshefte* **1984**, *6*, 272–282.
- Henn, U.; Schultz-Güttler, R. Review of some current coloured quartz varieties. *J. Gemmol.* **2012**, *33*, 29–43. [[CrossRef](#)]
- Paradise, J.R. The natural formation and occurrence of green quartz. *Gems Gemol.* **1982**, *18*, 39–42. [[CrossRef](#)]
- Hebert, L.B.; Rossmann, G. Greenish quartz from the Thunder Bay Amethyst Mine Panorama, Thunder Bay, Ontario, Canada. *Can. Min.* **2008**, *46*, 61–74. [[CrossRef](#)]
- McArthur, J.R.; Jennings, E.A.; Kissin, S.A.; Sherlock, R.L. Stable-isotope, fluid-inclusion, and mineralogical studies relating to the genesis of amethyst, Thunder Bay Amethyst Mine, Ontario. *Can. J. Earth Sci.* **1993**, *30*, 1955–1969. [[CrossRef](#)]
- Brooks, J. Marlborough Creek chrysoprase deposits, Rockhampton district, central Queensland. *Gems Gemol.* **1965**, *11*, 323–330.
- Visser, J. Nephrite and chrysoprase of Silesia. *Gemmologist* **1947**, *16*, 229–230.
- Sachanbinski, M.; Janeczek, J.; Platonov, A.; Rietmeijer, F.J.M. The origin of colour of chrysoprase from Szklary (Poland) and Sarykul Boldy (Kazakhstan). *N. Jahrb. Miner.* **2001**, *177*, 61–76. [[CrossRef](#)]
- Yang, L.; Mashkovtsev, R.I.; Botis, S.M.; Pan, Y. Multi-spectroscopic study of green quartzite (Guizhou Jade) from the Qinglong antimony deposit, Guizhou Province, China. *J. China Univ. Geosci.* **2007**, *18*, 327–329.
- Lieber, W. *Amethyst: Geschichte, Eigenschaften, Fundorte*; Christian Weise Verlag: München, Germany, 1994; 188p.
- Dedushenko, S.K.; Makhina, I.B.; Mar'in, A.A.; Mukhanov, V.A.; Perfiliev, Y.U.D. What oxidation state of iron determines the amethyst colour? *Hyperfine Interact.* **2004**, *156*, 417–422. [[CrossRef](#)]
- Di Benedetto, F.; Innocenti, M.; Tesi, S.; Romanelli, M.; D'Acapito, F.; Fornaciai, G.; Montegrossi, G.; Pardi, L.A. A Fe K-edge XAS study of amethyst. *Phys. Chem. Miner.* **2010**, *37*, 283–289. [[CrossRef](#)]
- SivaRamaiah, G.; Lin, J.; Pan, Y. Electron paramagnetic resonance spectroscopy of Fe³⁺ ions in amethyst: thermodynamic potentials and magnetic susceptibility. *Phys. Chem. Miner.* **2011**, *38*, 159–167. [[CrossRef](#)]
- Kievlenko, E.Y. *Geology of Gems*; Ocean Pictures Ltd.: Romsey, UK, 2003; 468p.
- Tatartinov, A.V. Silic Minerals and Amethyst formation Conditions in Skarn-Magnetite Fields of the South of Siberian Platform. In *Mineralogy and Genesis of East Siberia Gems*; Nauka: Novosibirsk, Russia, 1983; pp. 34–41. (In Russian)
- Flink, G. Bidrag till Sveriges mineralogy. *Arkiv Kemi. Mineral. Geol.* **1910**, *3*, 163–166.
- Geijer, P.; Magnusson, N.H. De mellansvenska järnmalmernas geologi. *Sver. Geol. Und.* **1944**, *35*, 558.
- Vogt, M. Serifos-die Mineralien-Insel in der griechischen Ägäis. *Lapis* **1991**, *16*, 26–37. (In German)
- Gauthier, G.; Albandakis, N. Minerals from the Serifos skarn, Greece. *Mineral. Rec.* **1991**, *22*, 303–308.
- Dibble, H.L. *Quartz: An Introduction to Crystalline Quartz*; Dibble Trust Fund Publ.: New York, NY, USA, 2002; 100p.
- Hyrsl, J.; Niedermayr, G. *Magic World: Inclusions in Quartz/Geheimnisvolle Welt: Einschlüsse im Quarz*; Bode Verlag GmbH: Haltern, Germany, 2003.
- Maneta, V.; Voudouris, P. Quartz megacrysts in Greece: Mineralogy and environment of formation. *Bull. Geol. Soc. Greece* **2010**, *43*, 685–696. [[CrossRef](#)]
- Voudouris, P.; Katerinopoulos, A. New occurrences of mineral megacrysts in tertiary magmatic-hydrothermal and epithermal environments in Greece. *Doc. Nat.* **2004**, *151*, 1–21.
- Ducoux, M.; Branquet, Y.; Jolivet, L.; Arbaret, L.; Grasemann, A.; Rabillard, C.; Gumiaux, C.; Drufin, S. Synkinematic skarns and fluid drainage along detachments: The West Cycladic Detachment System on Serifos Island (Cyclades, Greece) and its related mineralization. *Tectonophysics* **2017**, *695*, 1–26. [[CrossRef](#)]

32. Kronz, A.; van den Kerkhof, A.M.; Müller, A. Analysis of low element concentrations in Quartz by Electron Microprobe. In *Quartz: Deposits, Mineralogy, and Analytics*; Götze, J., Möckel, R., Eds.; Springer: New York, NY, USA, 2012; pp. 191–217.
33. Matthey, D.P. LaserPrep: An Automatic Laser-Fluorination System for Micromass “Optima” or “Prism” Mass Spectrometers. *Micromass Appl. Note* **1997**, *207*, 8.
34. Jolivet, L.; Brun, J.P. Cenozoic geodynamic evolution of the Aegean region. *Int. J. Earth Sci.* **2010**, *99*, 109–138. [[CrossRef](#)]
35. Ring, U.; Glodny, J.; Will, T.; Thomson, S. The Hellenic subduction system: high-pressure metamorphism, exhumation, normal faulting, and large-scale extension. *Annu. Rev. Earth Planet. Sci.* **2010**, *38*, 45–76. [[CrossRef](#)]
36. Jolivet, L.; Faccenna, C.; Huet, B.; Labrousse, L.; Le Pourhiet, L.; Lacombe, O.; Lecomte, E.; Burov, E.; Denèle, Y.; Brun, J.-P.; et al. Aegean tectonics: Strain localisation, slab tearing and trench retreat. *Tectonophysics* **2013**, *597–598*, 1–33. [[CrossRef](#)]
37. Maluski, H.; Bonneau, M.; Kienast, J.R. Dating the metamorphic events in the Cycladic area; ³⁹Ar/⁴⁰Ar data from metamorphic rocks of the Island of Syros (Greece). *Bull. Soc. Géol. Fr.* **1987**, *3*, 833–842.
38. Grasemann, B.; Petrakakis, K. Evolution of the Serifos metamorphic core complex. *J. Virtual Explor.* **2007**, *27*, 1–18. [[CrossRef](#)]
39. Rabillard, A.; Arbaret, L.; Jolivet, L.; Le Breton, N.; Gumiaux, C.; Augier, R.; Grasemann, B. Interactions between plutonism and detachments during metamorphic core complex formation, Serifos Island (Cyclades, Greece). *Tectonics* **2015**, *34*, 1080–1106. [[CrossRef](#)]
40. Schneider, D.A.; Senkowski, C.; Vogel, H.; Grasemann, B.; Iglseider, Ch.; Schmitt, A.K. Eocene tectonometamorphism on Serifos (western Cyclades) deduced from zircon depth-profiling geochronology and mica thermochronology. *Lithos* **2011**, *125*, 151–172. [[CrossRef](#)]
41. Salemink, J. On the Geology and Petrology of Serifos Island (Cyclades, Greece). *Annu. Geol. Pays Hell.* **1980**, *30*, 342–365.
42. Grasemann, B.; Schneider, D.A.; Stockli, D.F.; Iglseider, C. Miocene bivergent crustal extension in the Aegean: Evidence from the western Cyclades (Greece). *Lithosphere* **2012**, *4*, 23–39. [[CrossRef](#)]
43. Salemink, J. Skarn and Ore Formation at Serifos, Greece. Ph.D. Thesis, University of Utrecht, Utrecht, The Netherlands, 1985.
44. Stouraiti, C.; Baziotis, I.; Asimow, P.D.; Downes, H. Geochemistry of the Serifos calc-alkaline granodiorite pluton, Greece: Constraining the crust and mantle contributions to I-type granitoids. *Int. J. Earth Sci. (Geol. Rundsch)* **2018**, *107*, 1657. [[CrossRef](#)]
45. Sharp, Z.D.; Gibbons, J.A.; Maltsev, O.; Atudorei, V.; Pack, A.; Sengupta, S.; Shock, E.L.; Knauth, L.P. A calibration of the triple oxygen isotope fractionation in the SiO₂–H₂O system and applications to natural samples. *Geochim. Cosmochim. Acta* **2016**, *186*, 105–119. [[CrossRef](#)]
46. Taylor, H.P., Jr. Oxygen and hydrogen isotope relationships in hydrothermal mineral deposits. In *Geochemistry of Hydrothermal Ore Deposits*, 2nd ed.; Barnes, H.L., Ed.; Wiley: New York, NY, USA, 1979; pp. 236–318.
47. Giggenbach, W.F. The origin and evolution of fluids in magmatic-hydrothermal systems. In *Geochemistry of Hydrothermal Ore Deposits*, 3rd ed.; Barnes, H.L., Ed.; Wiley: New York, NY, USA, 1997; pp. 737–796.
48. Simmons, S.F.; Browne, P.R.L. Hydrothermal minerals and precious metals in the Broadlands-Ohaaki geothermal system: Implications for understanding low-sulfidation epithermal environments. *Econ. Geol.* **2001**, *95*, 971–999. [[CrossRef](#)]
49. Dana, J.D.; Dana, E.S.; Frondel, C. *The System of Mineralogy, Vol. 3: Silica Minerals*; John Wiley & Sons: New York, NY, USA, 1962.
50. Fournier, R.O. The behaviour of silica in hydrothermal solutions. Geology and geochemistry of epithermal systems. *Rev. Econ. Geol.* **1985**, *2*, 45–61.
51. Voudouris, P.; Melfos, V.; Mavrogonatos, C.; Tarantola, A.; Götze, J.; Alfieris, D.; Maneta, V.; Psimis, I. Amethyst occurrences in Tertiary volcanic rocks of Greece: Mineralogical, fluid inclusion and oxygen isotope constraints on their genesis. *Minerals* **2018**, *8*, 324. [[CrossRef](#)]

